

ARTICLES

Molecular Interactions in Lyotropic Reverse Hexagonal Liquid Crystals: A Dielectric Spectroscopy Study**Paul Ben Ishai,*† Dima Libster,‡ Abraham Aserin,‡ Nissim Garti,‡ and Yuri Feldman†***Department of Applied Physics and Casali Institute of Applied Chemistry, The Institute of Chemistry, Givat Ram Campus, The Hebrew University of Jerusalem, Jerusalem 91904, Israel**Received: March 4, 2009; Revised Manuscript Received: June 18, 2009*

A dielectric study of reverse hexagonal mesophases (H_{II}) is presented. Conducted in the frequency range 0.01–1 MHz and temperature range $293 < T < 319$ K, the study reveals complex molecular behavior in and around the interfaces of the mesoscopic structures of the gel. There exist three clearly defined dielectric relaxations related to separate moieties in the interface, as well as a temperature-activated dc conductivity. A critical temperature, $T_0 = 307$ K, is noted in the results and related to the dehydration of the glycerol monooleate (GMO) head groups. Effectively, this represents a breakdown of the interfacial layer of water. The consequences of this act are clearly visible in the change in behavior of the fitting parameters for all processes. A physical picture emerges whereby at $T_0 = 307$ K, the “loosening” of the GMO heads accentuates the dangling motion of the phosphatidylcholine (PC) tails, evidenced by counterion motion along the PC head. Furthermore, it precipitates the percolation of the large TAG molecules that are intercalated in the GMO and PC tails.

Introduction

The phase behavior of mixtures of glycerol monooleate (GMO) and water has lately attracted the attention of both the scientific and the applied research communities due to their potential utilization in pharmaceutical products^{1–4} and food systems.^{5,6} As a function of concentration and temperature, GMO and water can form a variety of lyotropic liquid crystals (LLCs), including lamellar (L_a), hexagonal (normal, H_I , or inverted H_{II}), and normal or inverted cubic (bicontinuous or micellar) structures.^{7–9}

Among these LLCs, the reverse hexagonal mesophases (H_{II}) are recently considered as very promising drug delivery vehicles, mainly owing to their unique structural features. The accepted scheme of an H_{II} mesophase is that of infinitely long, relatively straight, circular cylinders arranged in a two-dimensional array. Each cylinder is surrounded by a layer of surfactant molecules that are perpendicular to the cylindrical interface such that their hydrophobic moieties point outward the water rods.^{10–12} (Figure 1). These properties allow the H_{II} mesophases to entrap water-soluble compounds within the aqueous domains and hydrophobic molecules via direct interactions within their lipid hydrophobic compartments. The structural properties of the hexagonal mesophases composed of GMO/tricaprylin/water were extensively and systematically studied in our lab, mainly by SAXS, ATR-FTIR, SD-NMR, DSC, and rheological techniques, as was reported in our previous publications.^{13,14}

In addition, it was shown that phosphatidylcholine (PC) was solubilized into the ternary GMO/tricaprylin/water hexagonal

system.¹⁵ The incorporation of PC into the mesophases had a pronounced effect on the GMO–water interface region on the molecular level and improved the elastic properties and thermal stability of the H_{II} structures. It was also demonstrated using the ESEM technique that the surface topology of these systems possessed fractal characteristics, suggesting a discontinuous and disordered alignment of the corresponding internal water rods on the mesoscale.¹⁶ We as well revealed that the topography (a mesoscopic property) of the H_{II} phase was likely to be influenced by the microstructural parameters and the composition of the samples. This can potentially enhance transdermal drug delivery through the high surface area of these carriers owing to the tunable fractal nature of their surface.

Moreover, the practical feasibility of the solubilization of peptide drugs into the H_{II} mesophase was illustrated via the lipophilic drug cyclosporin A and hydrophilic desmopressin, and their entrapment effects on the phase and conformational changes within the phase were studied on a macroscopic scale¹⁵ and a molecular level.^{17,18}

Although the structural organization of hexagonal LLC is relatively well studied, the dynamic properties of these systems are not fully understood, so far. In this respect, dielectric spectroscopy (DS) is an extremely sensitive technique to explore intermolecular interactions and to monitor cooperative processes at the molecular level. It has been extensively applied to the molecular study of polymers,^{19,20} glass-formers,^{21,22} colloids,²³ and other systems to probe the aforementioned topics. Hexagonal LLCs are complex systems in which structural behavior is governed by both hydrogen bonds and van der Waals interactions. Consequently, they are expected to exhibit several relaxation processes. Monitoring different scales of molecular motion of these complex LLCs by DS would provide useful information about the behavior of the individual components of these materials, its bulk properties, and the interactions of

* Corresponding author address: The Applied Physics Department, The Selim and Rachel Benin School of Computer Science and Engineering, Givat Ram Campus, The Hebrew University of Jerusalem, Jerusalem 91904, Israel. Phone: 972-2-658-5061. E-mail: paulb@vms.huji.ac.il.

† Department of Applied Physics.

‡ Casali Institute of Applied Chemistry.

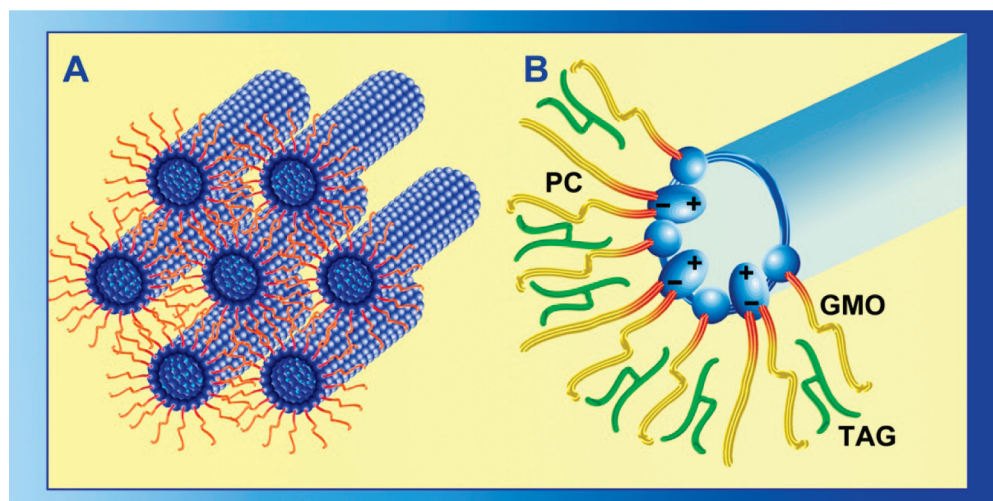


Figure 1. (A) Schematic presentation of the supramolecular organization of H_{II} mesophase, showing the cylinders' packing. (B) Schematic illustration focused on one cylinder of the mixed surfactant (GMO and PC) hexagonal system organization. Note that GMO and PC polar moieties are hydrated, but that TAG is located between the lipophilic chains of the surfactants.

the guest molecules with the mesophases. Cubic and lamellar GMO/water LLC has been investigated using dielectric analysis and oscillatory rheology by Bonacucina et al.²⁴ However, these measurements yielded distinct yet complementary and limited information on the dynamical behavior of the structures and the nature of the interactions between the liquid crystals and the drug. The dielectric behavior of simpler GMO/water systems was studied by He and Craig²⁵ as a function of temperature and water concentration. The authors noted in the dielectric spectra the various phase changes as conditions were modified and the data were fitted using equivalent circuit models. Such an approach is sensitive to variations in impedance between the component circuits. Consequently, they describe well domains and phase transitions, but they are not open to a molecular interpretation. State-of-the-art dielectric theory employs more advanced tools to explore the underlying physics of phenomenological fitting functions.^{26,27}

Hence, the present manuscript seeks to explore the dynamic behavior of H_{II} mesophases composed of GMO/tricaprylin/phosphatidylcholine/water on molecular and mesoscopic levels using dielectric spectroscopy and to establish a possible relationship between the dynamical and structural properties of these structures.

Materials and Methods

Monolein, GMO (OL type, molecular weight of 357 g mol⁻¹, density of 0.942 g ml⁻¹), distilled glycerol monooleate (min. 97 wt % monoglyceride), 2.5 wt % diglyceride and free glycerol 0.4 wt % (acid value 1.2, iodine value 68.0, melting point 37.5 °C) were obtained from Riken Vitamin Co. (Tokyo, Japan). Tricaprylin (TAG, molecular weight of 470.7 g mol⁻¹, density of 0.954 g ml⁻¹) (97–98 wt %) was purchased from Sigma Chemical Co. (St. Louis, MO). Phosphatidylcholine (molecular weight of 758 g mol⁻¹, density of 1.019 g ml⁻¹) of soybean origin (Epikuron 200, min. 92% PC) was purchased from Degussa (Hamburg, Germany). Water was double distilled. All ingredients were used without further purification.

Preparation of H_{II} Mesophases. The composition of 63 wt % GMO, 7 wt % tricaprylin (9:1 weight ratio), 10 wt % PC, and 20 wt % water was chosen for the preparation of the H_{II} mesophase. The GMO/PC/tricaprylin/water hexagonal liquid crystals were prepared by mixing weighed quantities of GMO, tricaprylin, and PC while heating to 80 °C. This was done in

sealed tubes under nitrogen atmosphere to avoid oxidation of the GMO and PC. An appropriate quantity of preheated water was added at the same temperature, and the samples were stirred and cooled to 25 °C. The samples were allowed to equilibrate for 24 h before examination.

Dielectric Spectroscopy Measurements. Dielectric measurements on the H_{II} mesophases were carried out in a relatively narrow temperature range, 293 < T < 319 K and in a frequency window 0.01 Hz < f < 1 MHz using a Novocontrol BDS 80 system (Novocontrol GmbH, Hamburg) based on an Alpha Dielectric Analyzer. The temperature control was provided by a Novocontrol Quatro Cryosystem (Novocontrol GmbH, Hamburg). The accuracy of the measurement in terms of $\tan \delta$ is <10⁻⁴.²⁸ The samples were mounted between two gold-plated electrode plates with a diameter of 24 mm. The plates were cleaned with alcohol and dried before the samples were placed. Teflon spacers of 1 mm thickness were used to maintain a constant and accurately known distance between the plate electrodes.

Results and Discussion

The temperature slices of the real component of complex dielectric permittivity, ϵ' , and the corresponding tan delta, $\tan(\delta) = \epsilon''/\epsilon'$, are shown in Figure 2 a and b as functions of temperature and frequency. Three distinct, thermally activated processes are noted (designated rather prosaically as processes 1, 2, and 3 in the figure) along with thermally activated dc conductivity. Process 1 exists in the higher frequency window (10⁵–10⁶ Hz) and has a clearly defined relaxation peak in the $\tan(\delta)$ representation. Process 2 is the most clearly defined of the processes, and its peak is in the frequency window 10²–10⁴ Hz. Both processes demonstrate a marked dependence on temperature. The lowest-frequency process, process 3, exhibits strong dielectric strengths and is situated on the lower frequency wing of the measurement window. It also demonstrates strong temperature dependence. In addition, there is a high-frequency tail, suggesting the presence of further dielectric relaxations outside the window of measurement, at frequencies above 1 MHz. A fitting function consisting of generic Havriliak–Negami (H–N) phenomenological functions²⁹ and a dc conductivity term was employed along with an in-house program, Matfit,³⁰ which is based on the scientific software Matlab,³¹ to fit the data.

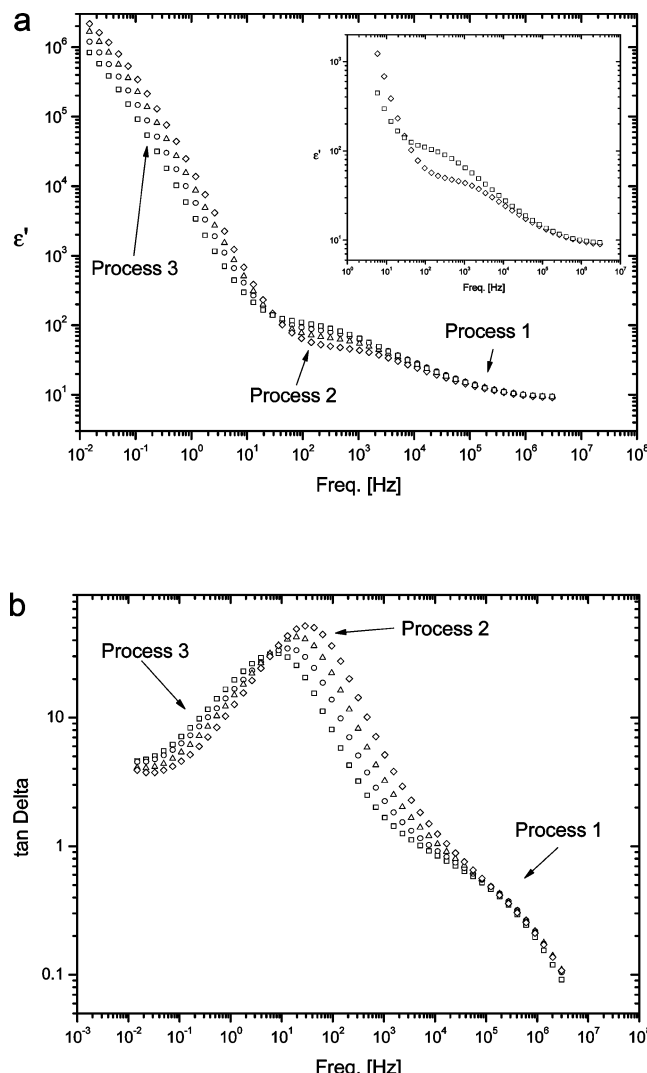


Figure 2. (a) Temperature slices of the real component of the dielectric permittivity as a function of frequency and (b) the same temperature slices in tan delta representation. Three activated processes are evident spanning the entire frequency range. The temperature slices are 293 (□), 303 (○), 311 (Δ), and 319 K (◇). The insert in panel a highlights process 1 and process 2 at 293 and 319 K for the higher frequencies.

$$\epsilon^*(\omega) - \epsilon_{hf} = \frac{-\sigma dc}{i\omega} + \sum_{n=1}^3 \frac{\Delta_{\epsilon_n}}{(1 + (i\omega\tau_n)^{\alpha_n})^{\beta_n}} \quad (1)$$

Where σ_{dc} is the dc conductivity, ϵ_{hf} is the high frequency value of the dielectric permittivity, Δ_{ϵ_n} is the dielectric strength, τ_n is the characteristic relaxation time for the process, and α_n and β_n are parameters ranging from 0 to 1. The challenge when fitting complex dielectric data is to concurrently deal with a number of simultaneous processes in the spectra. The task is simplified because the temperature behavior of the individual peaks is usually different. However, most procedures, while fitting both real and imaginary components simultaneously, do not relate to temperature as a variable but, rather, as a parameter. The Matfit program,³⁰ renamed DATAMA, was designed to address this problem by simultaneously fitting for all the temperature points. The smoothness of the solution is achieved through the addition of some penalty term to the cost function in the parameter minimization problem, together with a constraint condition for the total discrepancy measure between the data and fit function. The penalized functional approach is a well-

known regularization technique in image restoration problems, such as image denoising or image deblurring.³²

H–N functions have been found to be suitable phenomenological fits to describe complex, frequency-based dielectric data in many complex systems.³³ The specific case $\alpha_n = 1$, $\beta_n = 1$ gives the Debye relaxation law; the case $\beta_n = 1$, $\alpha_n < 1$ corresponds to the so-called Cole–Cole (CC) equation,³⁴ and the case $\alpha_n = 1$, $\beta_n < 1$ corresponds to the Cole–Davidson (CD) formula.³⁵ Although there is still some debate as to the meaning of the shape parameters α_n and β_n in the H–N function, the CC and CD cases can be given a microscopic interpretation.²⁶ Particularly, the CC equation can be demonstrated as arising from an interaction of the relaxing dipole moment with its underlying physical matrix.³⁶ The dipole–matrix interaction provides a restrictive component to the orientational relaxation of dipole in a Lorentzian mean field.

The presence of conductivity and the large dielectric strength of process 3 suggested that there is some kind of charge transport involving large apparent dipole moments. The microscopic model of the consequences of charge transport in dielectric behavior is well-explored in the time domain,³⁷ Accordingly, process 3 was then transformed to the time domain using the relationship

$$\psi(t) = L^{-1}(\epsilon(\omega)) \quad (2)$$

where L^{-1} is the inverse Laplace operator, and the time evolution of the system to a probing step field is described by the macroscopic correlation function, $\psi(t) = \langle M(0)M(t) \rangle / \langle M(0)M(0) \rangle$, where $M(0)$ is the macroscopic dipole moment at $t = 0$. The correlation function was further fitted using a power and stretch model.²⁶

$$\psi(t) = At^{-\mu} \exp\left[-\left(\frac{t}{\tau}\right)^\nu\right] \quad (3)$$

Here, A is the amplitude, τ is the characteristic relaxation time, and μ and ν are exponents ranging from 0 to 1. Equation 3 has been related to transport processes and, in particular, to percolation.²⁶ In this case, the thermal behavior of the exponent μ relates to the growth of cooperative clusters in the system in which charge or excitation transport may happen. Dielectric relaxation related to the cluster as a whole is manifested in a power behavior, $t^{-\mu}$. The exponent ν “stretches” the exponential behavior related to transport inside the cooperative cluster. The “stretching” is a consequence of the less than ideal media through which the transport occurs. Furthermore, the stretch parameter, ν , is related to the spatial fractal dimension, D_g , of the cluster by the relationship $D_g = 3\nu$.

The results are presented in Figures 2–6 for process 1, Figures 8–10 for process 2, Figures 11–13 for process 3, and Figure 14 for the dc conductivity. It should be noted that for processes 1 and 2, the shape parameter β in eq 1 was equal identically to 1, leading to so-called CC processes.²⁷

Any discussion of the dielectric relaxation behavior must, perforce, start with an understanding of the structure and role of the lipid layer surrounding the water rod. Although the mainstay is GMO with its nonionic headgroup and, consequently, H-bond interaction with the water interior, the PC with its zwitterionic tail is intercalated between them. TAG is intercalated between the hydrophobic tails¹⁷ (Figure 1). The layer is stabilized by interfacial water.¹⁶ Our previous studies^{16,17} indicated the critical role played by the lipid layer in the H_{II} mesophase’s ability to successfully

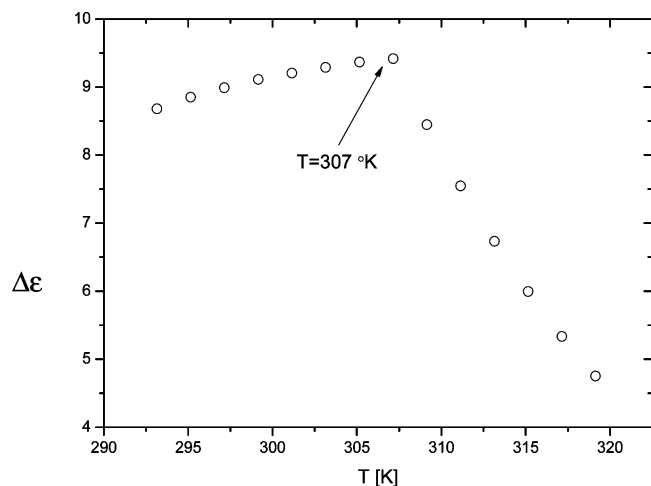


Figure 3. The dielectric strength of process 1. Evident is a critical temperature, $T = 307$ K, related to the dehydration of the GMO heads.

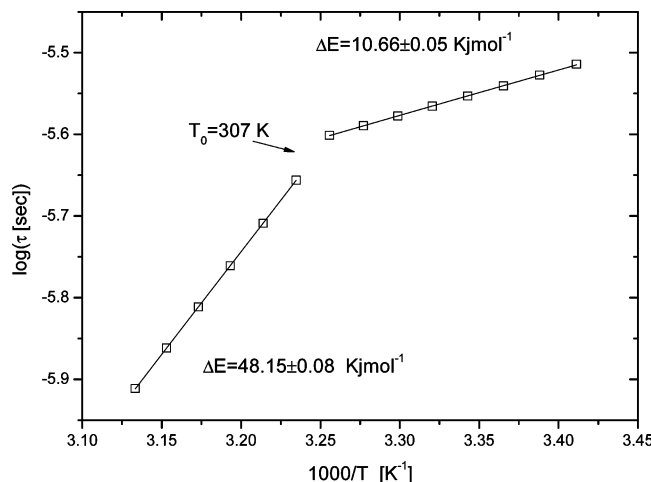


Figure 4. The characteristic relaxation times (\square) as a function of inverse temperature. The critical point $T = 307$ K is clearly visible, signaling a change in the energy of activation for the relaxation. The solid lines are the linear regression fittings from which the energies of activation were determined.

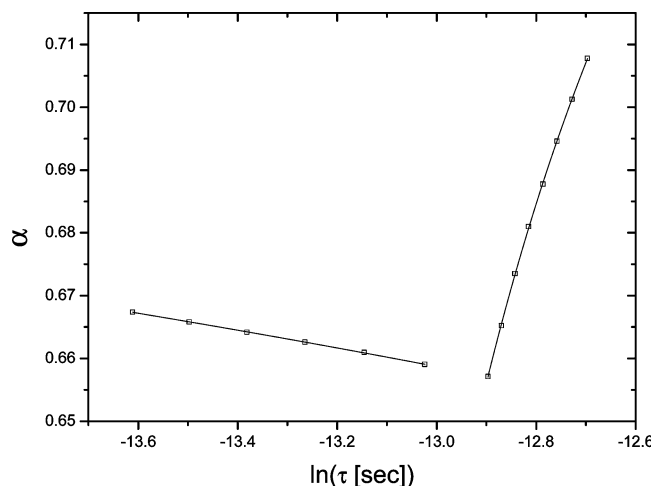


Figure 5. The stretch parameter, α , as a function of the characteristic time, τ . The solid lines are the fits according to eq 4.

carry a guest drug molecule. However, the release of the drug from the interior of the water rod (or from its tail) would be governed by the dynamics of the lipid layer. In the selected frequency range,²⁷

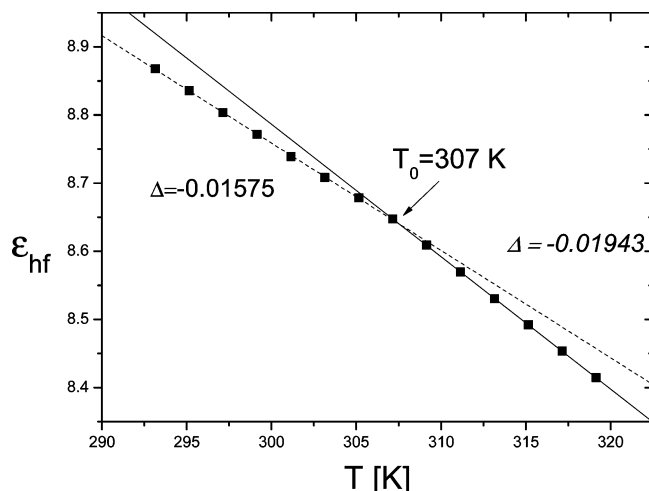


Figure 6. The high-frequency limit of the dielectric permittivity as a function of temperature. The solid and dashed lines are linear regression fits, and the gradients are listed by each accordingly.

relaxations relating to these membrane moieties should be evident. Furthermore, relaxations related directly to the water core would occupy higher frequency bands, not herein measured. Consequently, process 1, 2, and 3 are accordingly analyzed. With these considerations in mind, the results for each process are discussed below.

Process 1. The highest-frequency process, labeled process 1, is in a frequency range previously noted as characteristic of reorientations of the GMO polar headgroup.³⁸ The fitting parameters are illustrated in Figures 3–6. The dielectric strength (Figure 3) of process 1 reveals a critical temperature, $T_0 = 307$ K. Below $T_0 = 307$, there is an initial growth with increasing temperature that is indicative of a condensed state.³⁹ Above T_0 , the dielectric strength drops as the temperature increases. The temperature $T_0 = 307$ K has been recognized in NMR studies¹² as the beginning of a thermal dehydration of the GMO headgroup in the H_{II} mesophase. Therefore, above this critical point, the membrane is less stabilized by interfacial water, leading to a more “liquidlike” state, and consequently, the dielectric strength drops with increasing temperature. This “quasi” phase transition is reflected in the Arrhenius plot of the relaxation times against temperature. The energy of activation before T_0 is $\Delta E = 10.66 \pm 0.05$ kJ mol⁻¹. The complementary FTIR measurements¹⁷ showed that the β OH group (see Figure 7) is responsible for bonding between the neighboring GMO heads and is only moderately hydrated. For $T > T_0$, the activation energy for the GMO headgroup rotation increases to $\Delta E = 48.15 \pm 0.08$ kJ mol⁻¹. This suggests that the γ OH group, typically strongly hydrated, breaks away from the interfacial water layer and probably interacts with the carbonyl group (C=O) of GMO headgroups via intramolecular H-bonding. A final point of consideration is the shape parameter, α , derived from the CC equation. The $\alpha(\tau)$ dependences is indicative of the nature of dipole–matrix interaction. If the interactions of the dipole with its underlying physical matrix are indicated by a set of delta functions in an arbitrary time window, then the parameter α relates the microscopic characteristics of that interaction with the consequent dielectric response:³⁶

$$\alpha = \frac{D_g}{2} \frac{\ln(\tau\omega_0)}{\ln(\tau/\tau_0)} \quad (4)$$

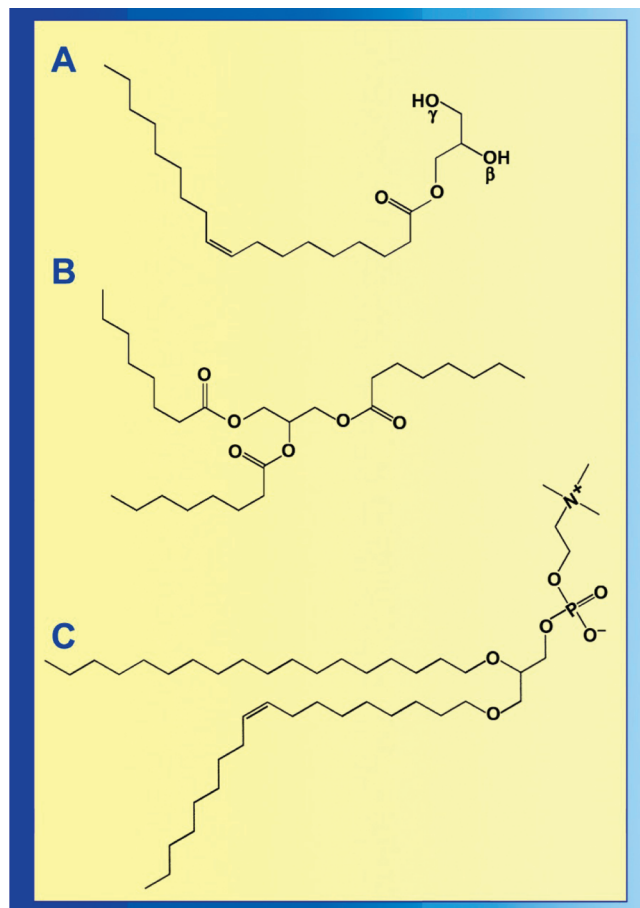


Figure 7. The constituents of the rods. (A) The GMO molecule. The γ OH group sits deep in the water core and is strongly hydrated. The β OH group is weakly hydrated but provides a mechanism to connect neighboring GMO heads. (B) The TAG molecule, which is intercalated between the hydrophobic tails of GMO and PC. The TAG dipole is weak (~ 2 D) and orientated along the molecule backbone. (C) The PC molecule with its polar head.

where D_g is the spatial fractal dimension in which the relaxation happens, τ_0 is a cutoff time scale for the relaxation process, and ω_0 is a characteristic frequency for the elemental act. For temperatures less than T_0 , the relevant values of eq 4 are $D_g = 1.79$ and $\tau_0 = 1.18 \times 10^{-6}$ s. For $T > T_0$, the relevant values are $D_g = 1.63$ and $\tau_0 = 0.071$ s. These values of the spatial fractal dimensions are indicative of relaxation happening in a layer.

Process 2. The frequency scales relating to process 2 (~ 10 kHz) have been recognized previously⁴⁰ as related to the tangential movement of counterions attached to the positive or negative charges of the PC at the hexagonal interface (see Figure 7). Other relaxation processes related to the PC would be outside the studied frequency window. Although PC presents the most probable cause, there is an anomaly. Relaxations of counterions are typically Arrhenius in nature, with a low energy of activation. The relaxation times are presented in Figure 8. It is clear that τ departs from Arrhenius behavior (an inset of the derivative of the Arrhenius plot shows the departure from a constant value for all temperature points, contrary to the expected result if the process exhibits Arrhenius behavior). However, process 2 does demonstrate Vogel–Fulcher–Tammann (VFT) behavior in its relaxation times (see Figure 8), typical for glass-forming liquids,²⁶ whereby the relaxation times follow the law

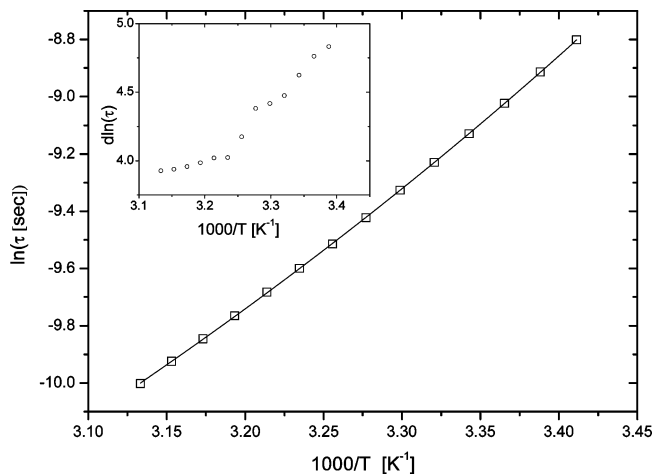


Figure 8. The Arrhenius plot for the relaxation times of process 2. The behavior is VFT (eq 5) in nature and demonstrates strong dielectric rigidity with a fragility index of 0.003 and $T_{VFT} = 189$ K. The inset shows the derivative of the logarithmic relaxation times. The deviation of the data from a constant value demonstrates clearly the non-Arrhenius nature of $\tau(T)$.

$$\ln(\tau) = \ln(\tau_0) + \frac{FT_{VFT}}{T - T_{VFT}} \quad (5)$$

where F is the fragility and T_{VFT} is a characteristic temperature at which τ diverges. For the process in question, $F = 0.03$ and $T_{VFT} = 189$ K. VFT has been recognized as indicative of cooperative processes^{41,42} involving clusterwise coupling. As proposed by G. Adam and J. Gibbs,⁴³ in glass-forming liquids, viscous flow occurs by cooperative rearrangements of clusters of particles. Each cluster is supposed to be acting independently of other similar clusters in the system, but it is assumed that the minimum size of such an independent cluster is temperature-dependent. This leads to $\tau = \tau_0 \exp(A/TS_c)$, where A is a constant and S_c is the configurational entropy. If S_c goes to zero at a finite temperature (i.e., $S_c = a[(T - T_k)/T]$, where T_k is the temperature representing the minimum in configurational entropy of the system under investigation), the VFT equation is obtained with $T_{VFT} = T_k$.

Yet counterion relaxation should be on the level of the unit dipole only, resulting in a cumulative process and in Arrhenius behavior in the relaxation times. A possible solution could be that the counterion relaxation acts as a label for the cooperative behavior of the hydrophobic tails. The ability of PC to stabilize the GMO/TAG/water interface was noted in ref 15. This “stiffening” of the interface implies a degree of cooperation between the PC molecules and their surroundings, leading to “dangling” of the PC tails in a weakly cooperative fashion. The interaction between the counterion and the PC head arises because of Coulombic interactions only. Dangling of the PC tails leads to a similar fluctuation in the PC head, perturbing the Coulombic interaction of the head with the counterion and leading to a manifestation of VFT behavior in what should be a purely thermal process. Fragility implies a structural sensitivity of the liquid to temperature.⁴² Liquids with high fragility exhibit many paths leading to coupling between relaxing units. Consequently, an excess of configurational entropy is involved which can be manifested in a deviation from Arrhenius behavior. Hydrophobic tails interacting by short-range van der Waals forces have a limited number of paths available to them; practically, only via nearest neighbors. Therefore, it is to be expected that their fragility would be accordingly small. T_{VFT}

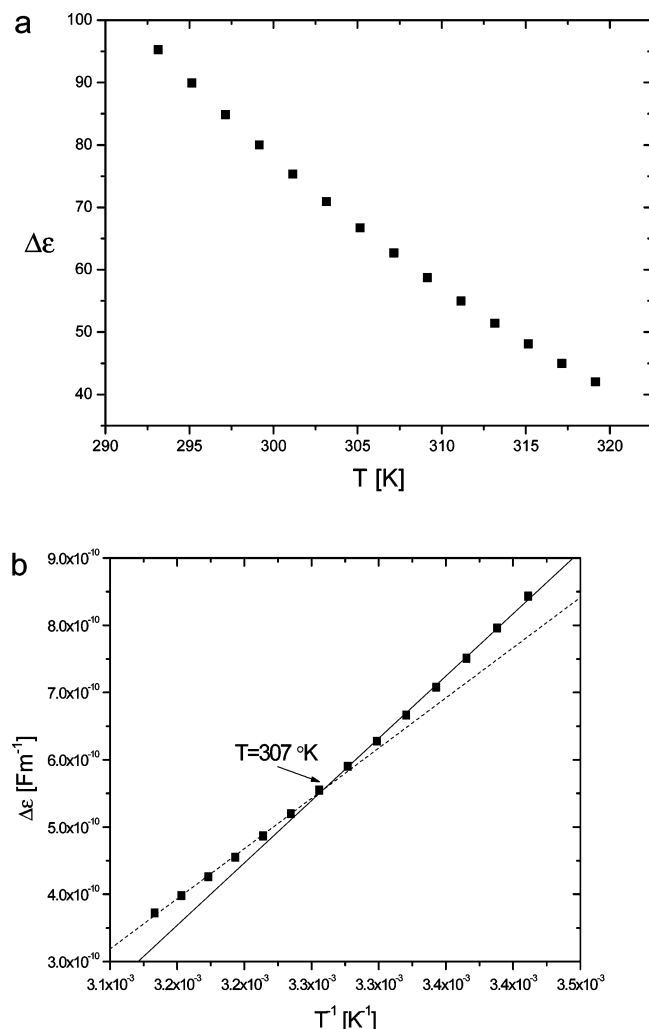


Figure 9. (a) The dielectric strength as a function of temperature for process 2. It is a monotonically decreasing function, in line with liquid behavior. (b) A reciprocal plot of the dielectric strength reveals a dependence on $T_0 = 307$ K. The dashed and solid lines are linear regression fits above and below T_0 , respectively.

is often noted as close to the glass-forming temperature of the system.⁴¹ However, the complex structure of the mesophase is not stable at such temperatures.

The critical temperature, $T_0 = 307$ K, is not noted in the relaxation times; however, a careful examination of the dielectric strength demonstrates a dependence on T_0 (see Figure 9b). The phenomenological form of the dependence is $\Delta\epsilon = A/T$, which is proportional to the number of dipoles involved,²⁷

$$\Delta\epsilon = \frac{A}{T} \propto \frac{N\mu^2}{kT} \quad (6)$$

where N is the number of dipoles, μ is the dipole moment, and k is Boltzmann's constant. From Figure 9b, $A = (1.49 \pm 0.03) \times 10^{-6}$ F K m\$^{-1}\$ for $T > T_0$ and $A = (1.85 \pm 0.03) \times 10^{-6}$ F K m\$^{-1}\$ for $T < T_0$. The dielectric strength is a complicated function depending on a number of factors, including dipole–dipole interaction terms, dipole–local field terms, and the thermodynamic state of the dipole set. To quantitatively exploit it, one should adopt approaches such as the Kirkwood correlation factor²⁷ or Frölich's formula.²⁷ However, if one is interested in a qualitative evaluation only, then one can ignore local field effects and possible dipole–dipole interactions and use the result of

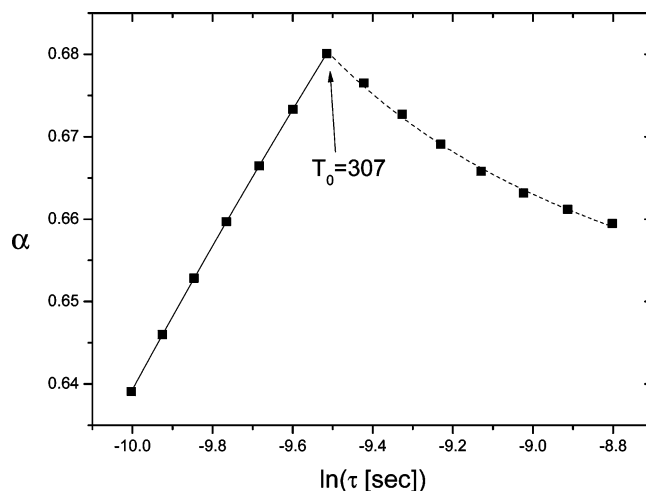


Figure 10. $\alpha(\tau)$ dependences for process 2 according to eq 4. The dashed and solid lines are the fit according to eq 4. There is a dramatic change in behavior at $T_0 = 307$ K. In particular, the spatial fractal dimensions indicate that the relaxation moves from occurring in the bulk volume ($D_g = 2.59$) to occurring in layers ($D_g = 1.26$).

eq 6 as a first approximation. In this case, a direct interpretation of the dielectric strength in terms of the known PC concentration leads to a conundrum. The estimated dipole moment is on the order of 10^6 Debye units, a figure unreasonable for counterion shielding on the PC head. But if this dipole moment is converted to a length scale, then a single charge separation would be on the micrometer scale, similar to the length scale of the water rods.¹⁶ It is possible to assume an apparent dipole, formed by a charge imbalance between the ends of a rod. The movement of a counterion along the PC head in the rod membrane would be sufficient to induce an orientational change in the apparent dipole. The time scale for such an orientational change is dictated by charge transfer between neighboring zwitterionic heads. The motivation for an ion jump from one PC head to another would be linked to cooperative fluctuations (dangling) within the hydrophilic tails, manifested in a similar fluctuation of the PC head.

Because the gradient A in eq 6 is proportional to the number of dipoles involved in the process, the decrease noted in its value when $T > T_0$ could be interpreted as a decrease in the number of apparent dipoles, stemming from a loosening of the PC ionic heads and a disruption of counterion movement. The T_0 dependence is more pronounced for $\alpha(\tau)$, as illustrated in Figure 10. Using the formulism of eq 4, the fitting results suggest a spatial fractal dimension, $D_g = 2.59 \pm 0.06$ before T_0 and 1.26 ± 0.01 afterward. These values are consistent with a relaxation throughout the volume bulk before T_0 and in layers after T_0 . It should be noted that the derived value of the spatial fractal dimension concurs with that found by ESEM¹⁶ measurements for 20% water ($D_s = 2.3$) at room temperature, further confirming this process as relating to the rods themselves.

Process 3. Process 3 demonstrates the existence of the critical temperature, $T_0 = 307$ K, in the amplitude (Figure 11), placing it in the vicinity of the interface. Coupled with its power and stretch behavior (eq 3), it would suggest a percolative process, as does the increase in the relaxation times (Figure 12) with temperature. Yet typically approaching the percolation threshold, the thermal behavior of the exponents μ and ν is the reverse of Figure 13. In fact, they are more reminiscent of a network in the immediate aftermath of its percolation threshold. If it is ionic percolation in the water interior, then the conductivity exhibits a characteristic S curve with its point of inflection centered on

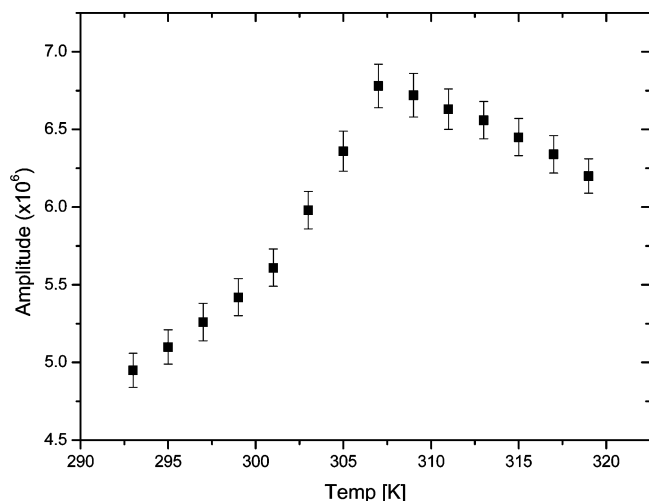


Figure 11. The amplitude of process 3. The critical point, $T_0 = 307$ K, is clearly visible and indicates a change in the nature of the relaxation. Before T_0 , the amplitude is reminiscent of a percolative process before the onset of percolation.

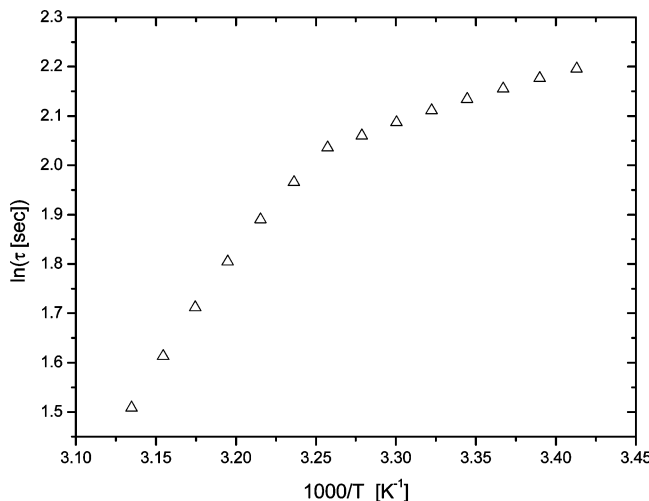


Figure 12. The relaxation times for process 3 derived from fitting eq 3 to the dielectric data for process 3 in the time domain.

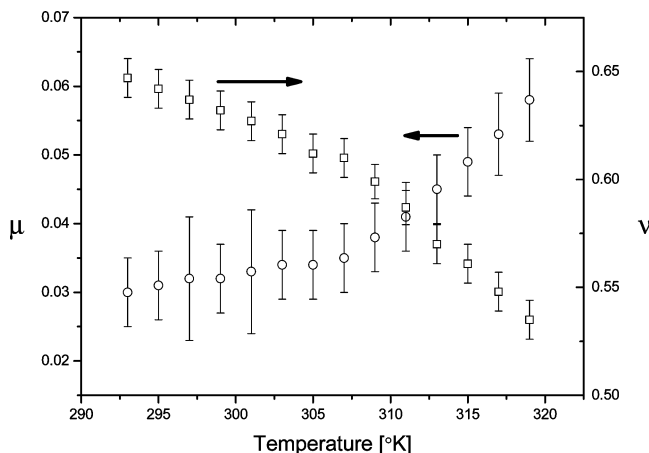


Figure 13. The power, μ , and stretch, ν , parameters of process 3 derived from the fitting of eq 3 to the data for process 3. The arrows indicate the relevant axis.

the percolation threshold temperature, but in this case, the dc conductivity is Arrhenius (Figure 14) in behavior, ruling out an ionic mechanism. Another possibility is proton percolation through a H-bond network. However, this occurs at much higher

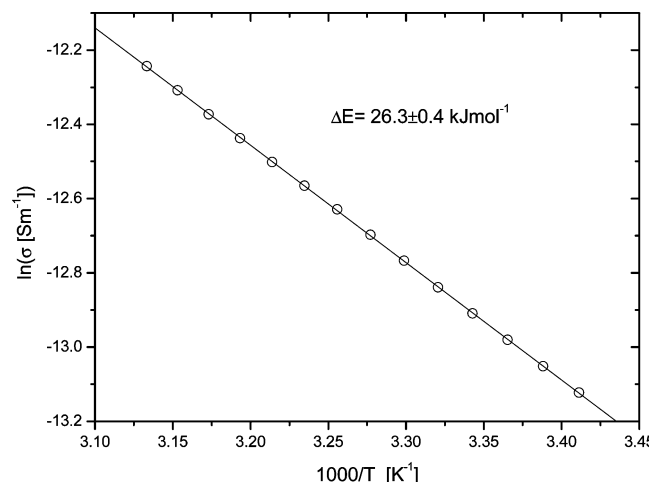


Figure 14. The dc conductivity in an Arrhenius plot. The derived energy of activation is indicated on the graph.

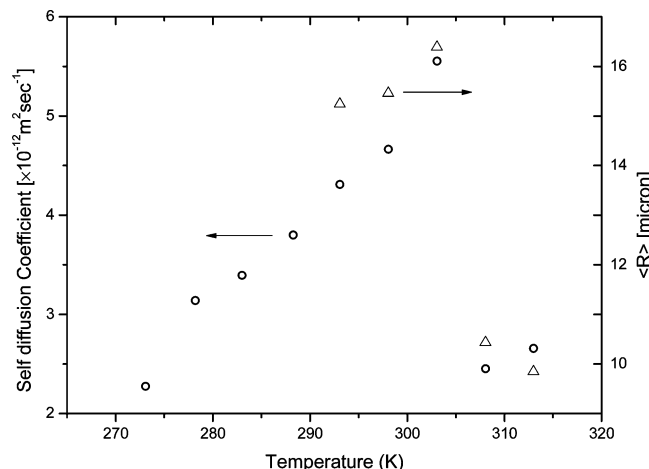


Figure 15. The self-diffusion coefficient of TAG intercalated between the GMO tails (o) and the calculated mean square displacement (Δ).

frequencies than those measured.⁴⁴ The only other unaccounted dipole in the system resides in the TAG molecule. TAG is intercalated between the tails of GMO and PC and possesses a dipole moment of ~ 2 D.⁴⁵ Self-diffusion NMR measurements of the system demonstrate the increase in the diffusion coefficient of TAG as the temperature increases¹² (Figure 15) toward $T = 307$ K. This is consistent with a percolation view of the dielectric behavior of process 3. We can conceive the following hypothesis (illustrated in Figure 16): Due to Coulombic interactions with the zwitterionic PC headgroup, the vector of the dipole moment of the TAG molecule is most likely orientated radially from the interface surface. However, as demonstrated by SD-NMR,¹² the TAG is only loosely bound to the lipophilic tails and, consequently, can percolate through the dangling tails. This interpretation is further strengthened by the shift in the C—O stretching vibration mode of TAG in FTIR measurements.¹⁷ In this case, the addition of PC shifted this band to lower wave numbers, indicating competition is taking place between the PC and TAG molecules for the solvation of the GMO tails. Consequently, part of the triglyceride molecules are “salted out” in favor of the PC–GMO interactions. A similar competition for the solvation of GMO tails was noted when vitamin E or vitamin E acetate was incorporated in H_{II} with and without TAG.⁴⁶ As a further consequence, the perturbation to the PC would lead to the counterion movement noted in process 2. At $T = 307$ K, the detachment of interfacial water from the GMO

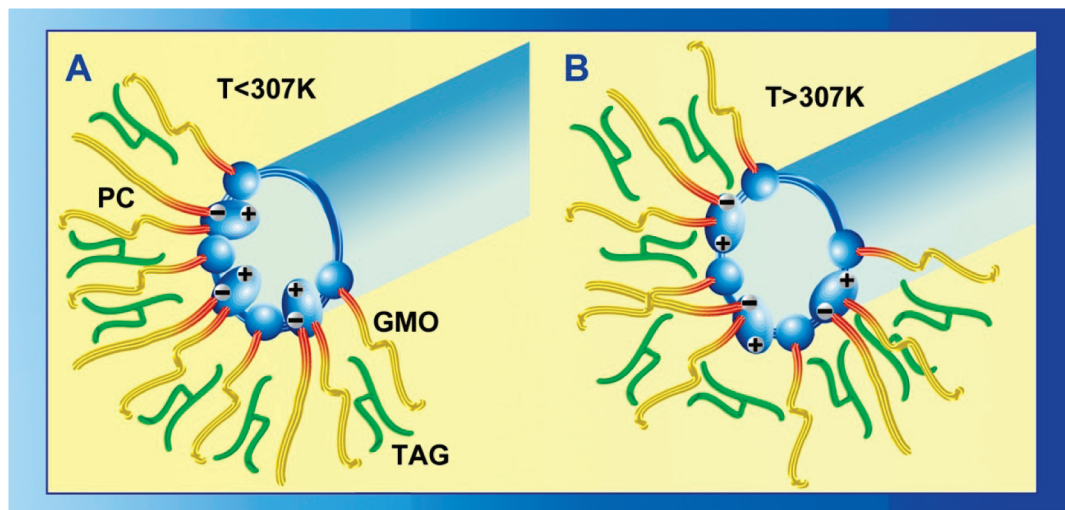


Figure 16. (A) Below $T = 307\text{ K}$, interfacial water stabilizes the lipid layer via its interaction with the GMO head $\gamma\text{ OH}$ group. Consequently, the Tag molecule remains intercalated between the tails. Dangling tails of the PC group give rise to counterion movement and also TAG dipolar relaxation. (B) Above $T = 307\text{ K}$, the interface is destabilized by the breakdown of the interfacial water layer. The perturbation of the PC heads leads to greater dangling, enabling diffusive movement of the TAG molecule through the tails.

heads would lead to a strengthening of the interaction of the TAG dipole moment with GMO, leading to a reduction in its diffusion constant (see Figure 15). In addition, after $T = 307\text{ K}$, the relaxation times show a stronger thermal activation, as expressed by the sharp increase in the gradient of the Arrhenius plot (Figure 12). The expression for mean square displacement in self-diffusion is

$$R^2 = 2d_E D \tau \quad (7)$$

where d_E is the Euclidian dimension, D is the self-diffusion constant, and τ is the relaxation time. Using eq 7 and the self-diffusion constant of TAG, the derived mean square displacements are shown in Figure 15, and they are in the region of micrometers, a reasonable figure for such systems.⁴⁷ This, coupled with the perturbation on the PC head, would lead to a large apparent dipole moment and can account for the large strength of the process. Although the similarity in behavior of the mean square displacement and the diffusion constant lends credence to this hypothesis, a full exploration of the TAG-PC interaction will be presented elsewhere.

Conclusion

The interfacial region of the H_{II} mesophase is revealed as a complex colloid metamaterial stabilized by interfacial water. The picture illuminated by our earlier measurements concerning the structural aspects of hexagonal mesophases was confirmed by dielectric spectroscopy. However, the kinetic aspects of the interface are probed for the first time. They reveal the critical role played by interfacial water in stabilizing the interface. In some ways, it is possible to envisage the water core a backbone, carrying its lipid layer. Although not herein investigated, it remains to be seen how the T_0 depends on the composition of the interface. For the first time, we have observed cooperative behavior of the lipophilic tails. This is not a usual occurrence because the tails are largely transparent to DS. The role played by the interaction of the PC ionic headgroups with the large TAG molecule is recognized as responsible for the major elements of dielectric behavior. It is still to be investigated to what level the dissociation of interfacial water is affected by the PC-TAG interaction. Such investigations will lead to the

ability to plan critical behavior of the interface and raises the possibility of fine-tuning the material for particular operations, such as drug release at certain times only. These and other avenues of research and application will be investigated in the future.

References and Notes

- Boyd, B. J.; Whittaker, D. V.; Khoo, S.; Davey, G. *Int. J. Pharm.* **2006**, *318*, 154–162.
- Lynch, M. L.; Ofori-Boateng, A.; Hippe, A.; Kochvar, K.; Spicer, P. T. *J. Colloid Interface Sci.* **2003**, *260*, 404–413.
- Lopes, L. B.; Speretta, F. F.; Bentley, M. V. L. *Eur. J. Pharm. Sci.* **2007**, *32*, 209–215.
- Boyd, B. J.; Khoo, S.; Whittaker, D. V.; Davey, G.; Porter, C. J. *Int. J. Pharm.* **2007**, *340*, 52–60.
- Sagalowicz, L.; Leser, M.; Watzke, H.; Michel, M. *Trends Food Sci. Technol.* **2006**, *17*, 204–214.
- Sagalowicz, L.; Mezzenga, R.; Leser, M. E. *Curr. Opin. Colloid Interface Sci.* **2006**, *11*, 224–229.
- Larsson, K. *J. Phys. Chem.* **1989**, *93*, 7304–7314.
- Qiu, H.; Caffrey, M. *Biomaterials* **2000**, *21*, 223–234.
- Yamashita, J.; Shiono, M.; Hato, M. *J. Phys. Chem. B* **2008**, *112*, 12286–12296.
- Amar-Yuli, I.; Garti, N. *Colloids Surf., B* **2005**, *43*, 72–82.
- Amar-Yuli, I.; Wachtel, E.; Ben Shoshan, E.; Danino, D.; Aserin, A.; Garti, N. *Langmuir* **2007**, *23*, 3637–3645.
- Amar-Yuli, I.; Wachtel, E.; Shalev, D.; Moshe, H.; Aserin, A.; Garti, N. *J. Phys. Chem. B* **2007**, *111*, 13544–13553.
- Amar-Yuli, I.; Wachtel, E.; Shalev, D.; Aserin, A.; Garti, N. *J. Phys. Chem. B* **2008**, *112*, 3971–3982.
- Amar-Yuli, I.; Aserin, A.; Garti, N. *J. Phys. Chem. B* **2008**, *112*, 10171–10180.
- Libster, D.; Aserin, A.; Wachtel, E.; Shoham, G.; Garti, N. *J. Colloid Interface Sci.* **2007**, *308*, 514–524.
- Libster, D.; Ben Ishai, P.; Aserin, A.; Shoham, G.; Garti, N. *Langmuir* **2008**, *24*, 2118–2127.
- Libster, D.; Ishai, P. B.; Aserin, A.; Shoham, G.; Garti, N. *Int. J. Pharm.* **2009**, *367*, 115–126.
- Libster, D.; Aserin, A.; Yariv, D.; Shoham, G.; Garti, N. *J. Phys. Chem. B*, submitted.
- Runt, J. P.; Fitzgerald, J. J. *Dielectric Spectroscopy of Polymeric Materials: Fundamentals and Applications*; American Chemical Society: Washington, DC, **1997**.
- Adachi, K.; Kotaka, T. *Prog. Polym. Sci.* **1993**, *18*, 585–622.
- Goldstein, M. A. R. S. *The Glass Transition and the Nature of the Glassy State*; New York Academy of Sciences: New York, NY, **1976**.
- Richert, R.; Blumen, A. *Disorder Effects on Relaxational Processes*; Springer-Verlag GmbH & Co.: Berlin, Heidelberg, **1994**.
- Sjöblom, J. *Encyclopedic Handbook of Emulsion Technology*, 1st ed.; CRC Press: Boca Raton, FL, **2001**.
- Bonacucina, G.; Palmieri, G.; Craig, D. *J. Pharm. Sci.* **2005**, *94*, 2452–2462.

- (25) He, R.; Craig, D. *J. Phys. Chem. B* **1998**, *102*, 1781–1786.
- (26) Feldman, Y.; Puzenko, A.; Ryabov, Y. In *Advances in Chemical Physics, Part A, Fractals, Diffusion and Relaxation in Disordered Complex Systems*; John Wiley & Sons: New York, **2006**; Vol. 133, pp 1–125.
- (27) Kremer, F.; Schönhals, A. *Broadband Dielectric Spectroscopy*, 1st ed.; Springer, New York, Berlin, **2002**.
- (28) User's Manual "Alpha High Resolution dielectric Analyser"; Novocontrol GmbH: Hundsangen, Germany, 2000.
- (29) Havriliak, S.; Negami, S. *J. Polym. Sci., Part C* **1966**, *99*.
- (30) Axelrod, N.; Axelrod, E.; Gutina, A.; Puzenko, A.; Ben Ishai, P.; Feldman, Y. *Meas. Sci. Technol.* **2004**, *15*, 755–764.
- (31) Matlab; The MathWorks Inc.: Natick, MA, 2008.
- (32) Verveer, P. J.; Gemkow, M. J.; Jovin, T. M. *J. Microsc.* **1999**, *193*, 50–61.
- (33) Böttcher, C. J. F. *Theory of Electric Polarization: Dielectrics in Time-Dependent Fields*, 2nd ed.; Elsevier Science Ltd.: Amsterdam, The Netherlands; New York, **1980**.
- (34) Cole, K. S.; Cole, R. H. *J. Chem. Phys.* **1941**, *9*, 341–351.
- (35) Davidson, D.; Cole, R. H. *J. Chem. Phys.* **1951**, *19*, 1484–1490.
- (36) Ryabov, Y. E.; Feldman, Y. *Phys. A* **2002**, *314*, 370–378.
- (37) Jonscher, A. K. *Universal Relaxation Law*; Chelsea Dielectrics P.: London, **1995**.
- (38) Crawford, G.; Earnshaw, J. *Biophys. J.* **1987**, *52*, 87–94.
- (39) Schlosser, E.; Schonhals, A.; Carius, H.; Goering, H. *Macromolecules* **1993**, *26*, 6027–6032.
- (40) Ermolina, I.; Smith, G.; Ryabov, Y.; Puzenko, A.; Polevaya, Y.; Nigmatullin, R.; Feldman, Y. *J. Phys. Chem. B* **2000**, *104*, 1373–1381.
- (41) Angell, C. *Science* **1995**, *267*, 1924–1935.
- (42) Green, J.; Ito, K.; Xu, K.; Angell, C. *J. Phys. Chem. B* **1999**, *103*, 3991–3996.
- (43) Adam, G.; Gibbs, J. *J. Chem. Phys.* **1965**, *43*, 139–146.
- (44) Krasnolohovets, V.; Tomchuk, P.; Lukyanets, S. *Adv. Chem. Phys.* **2003**, *125*, 351–548.
- (45) Ivanova, T.; Mircheva, K.; Dobrev, G.; Panaiotov, I.; Proust, J.; Verger, R. *Colloids Surf., B* **2008**, *63*, 91–100.
- (46) Amar-Yuli, I.; Aserin, A.; Garti, N. *J. Phys. Chem. B* **2008**, *112*, 10171–10180.
- (47) Wennerström, H.; Söderman, O.; Olsson, U.; Lindman, B. *Colloids Surf. A* **1997**, *123–124*, 13–26.

JP901987P